CHAPTER

1

CLASSICAL NMR SPECTROSCOPY

The explosive growth in the field of nuclear magnetic resonance (NMR) spectroscopy that continues today originated with the development of pulsed Fourier transform NMR spectroscopy by Ernst and Anderson (*1*) and the conception of multidimensional NMR spectroscopy by Jeener (*2, 3*). Currently, NMR spectroscopy and x-ray crystallography are the only techniques capable of determining the three-dimensional structures of macromolecules at atomic resolution. In addition, NMR spectroscopy is a powerful technique for investigating time-dependent chemical phenomena, including reaction kinetics and intramolecular dynamics. Historically, NMR spectroscopy of biological macromolecules was limited by the low inherent sensitivity of the technique and by the complexity of the resultant NMR spectra. The former limitation has been alleviated partially by the development of more powerful magnets and more sensitive NMR spectrometers and by advances in techniques for sample preparation (both synthetic and biochemical). The latter limitation has been transmuted into a significant advantage by the phenomenal advances in the theoretical and experimental capabilities of NMR spectroscopy (and spectroscopists). The history of these developments has been reviewed by Ernst and by Wüthrich in their 1991 and 2002 Nobel Laureate lectures, respectively (*4, 5*). In light of subsequent developments, the conclusion of Bloch's

initial report of the observation of nuclear magnetic resonance in water proved prescient: "We have thought of various investigations in which this effect can be used fruitfully" (*6*).

1.1 Nuclear Magnetism

Nuclear magnetic resonances in bulk condensed phase were reported for the first time in 1946 by Bloch et al. (*6*) and by Purcell et al. (*7*). Nuclear magnetism and NMR spectroscopy are manifestations of nuclear spin angular momentum. Consequently, the theory of NMR spectroscopy is largely the quantum mechanics of nuclear spin angular momentum, an intrinsically quantum mechanical property that does not have a classical analog. The physical origins of the nuclear spin angular momentum are complex, but have been discussed in review articles (*8, 9*). The spin angular momentum is characterized by the nuclear spin quantum number, I. Although NMR spectroscopy takes the nuclear spin as a given quantity, certain systematic features can be noted: (*i*) nuclei with odd mass numbers have half-integral spin quantum numbers, (*ii*) nuclei with an even mass number and an even atomic number have spin quantum numbers equal to zero, and (*iii*) nuclei with an even mass number and an odd atomic number have integral spin quantum numbers. Because the NMR phenomenon relies on the existence of nuclear spin, nuclei belonging to category (*ii*) are NMR inactive. Nuclei with spin quantum numbers greater than 1/2 also possess electric quadrupole moments arising from nonspherical nuclear charge distributions. The lifetimes of the magnetic states for quadrupolar nuclei in solution normally are much shorter than are the lifetimes for nuclei with $I = 1/2$. NMR resonance lines for quadrupolar nuclei are correspondingly broad and can be more difficult to study. Relevant properties of nuclei commonly found in biomolecules are summarized in Table 1.1. For NMR spectroscopy of biomolecules, the most important nuclei with $I = 1/2$ are ^{1}H, ^{13}C, ^{15}N, ^{19}F, and ^{31}P; the most important nucleus with $I = 1$ is the deuteron (^{2}H).

The nuclear spin angular momentum, **I**, is a vector quantity with magnitude given by

$$|\mathbf{I}| = [\mathbf{I} \cdot \mathbf{I}]^{1/2} = \hbar[I(I+1)]^{1/2}, \qquad [1.1]$$

in which I is the nuclear spin angular momentum quantum number and $\hbar$ is Planck's constant divided by 2π. Due to the restrictions of quantum mechanics, only one of the three Cartesian components of **I** can be

TABLE 1.1
Properties of selected nuclei[a]

Nucleus	I	γ $(\mathrm{T\,s})^{-1}$	Natural abundance (%)
^{1}H	1/2	2.6752×10^{8}	99.99
^{2}H	1	4.107×10^{7}	0.012
^{13}C	1/2	6.728×10^{7}	1.07
^{14}N	1	1.934×10^{7}	99.63
^{15}N	1/2	-2.713×10^{7}	0.37
^{17}O	5/2	-3.628×10^{7}	0.038
^{19}F	1/2	2.518×10^{8}	100.00
^{23}Na	3/2	7.081×10^{7}	100.00
^{31}P	1/2	1.0839×10^{8}	100.00
^{113}Cd	1/2	-5.961×10^{7}	12.22

[a]Shown are the nuclear spin angular momentum quantum number, I, the magnetogyric ratio, γ, and the natural isotopic abundance for nuclei of particular importance in biological NMR spectroscopy.

specified simultaneously with $\mathbf{I}^2 \equiv \mathbf{I} \cdot \mathbf{I}$. By convention, the value of the z-component of $\mathbf{I}$ is specified by the following equation:

$$I_z = \hbar m, \tag{1.2}$$

in which the magnetic quantum number $m = (-I, -I+1, \ldots, I-1, I)$. Thus, I_z has $2I+1$ possible values. The orientation of the spin angular momentum vector in space is quantized, because the magnitude of the vector is constant and the z-component has a set of discrete possible values. In the absence of external fields, the quantum states corresponding to the $2I+1$ values of m have the same energy, and the spin angular momentum vector does not have a preferred orientation.

Nuclei that have nonzero spin angular momentum also possess nuclear magnetic moments. As a consequence of the Wigner–Eckart theorem (*10*), the nuclear magnetic moment, $\boldsymbol{\mu}$, is collinear with the vector representing the nuclear spin angular momentum vector and is defined by

$$\begin{aligned} \boldsymbol{\mu} &= \gamma \mathbf{I}, \\ \mu_z &= \gamma I_z = \gamma \hbar m, \end{aligned} \tag{1.3}$$

in which the magnetogyric ratio, γ, is a characteristic constant for a given nucleus (Table 1.1). Because angular momentum is a quantized

property, so is the nuclear magnetic moment. The magnitude of γ, in part, determines the receptivity of a nucleus in NMR spectroscopy. In the presence of an external magnetic field, the spin states of the nucleus have energies given by

$$E = -\boldsymbol{\mu} \cdot \mathbf{B}, \qquad [1.4]$$

in which **B** is the magnetic field vector. The minimum energy is obtained when the projection of μ onto **B** is maximized. Because $|\mathbf{I}| > I_z$, $\boldsymbol{\mu}$ cannot be collinear with **B** and the m spin states become quantized with energies proportional to their projection onto **B**. In an NMR spectrometer, the static external magnetic field is directed by convention along the z-axis of the laboratory coordinate system. For this geometry, [1.4] reduces to

$$E_m = -\gamma I_z B_0 = -m\hbar\gamma B_0, \qquad [1.5]$$

in which B_0 is the static magnetic field strength. In the presence of a static magnetic field, the projections of the angular momentum of the nuclei onto the z-axis of the laboratory frame results in $2I+1$ equally spaced energy levels, which are known as the Zeeman levels. The quantization of I_z is illustrated by Fig. 1.1.

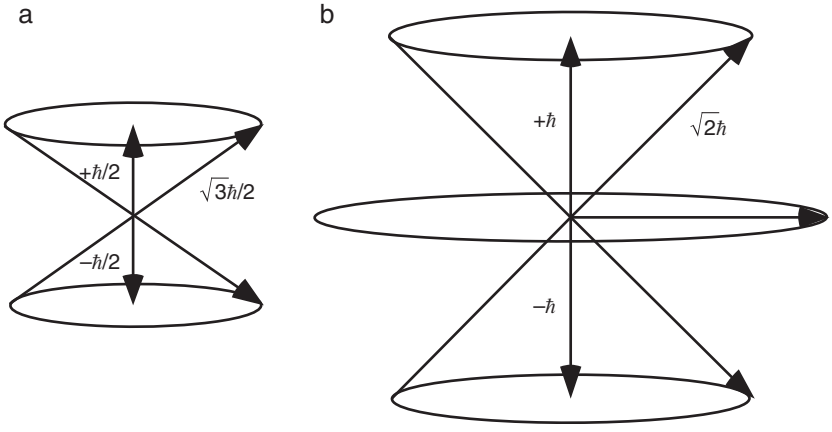

FIGURE 1.1 Angular momentum. Shown are the angular momentum vectors, **I**, and the allowed z-components, I_z, for (a) a spin-1/2 particle and (b) a spin-1 particle. The location of **I** on the surface of the cone cannot be specified because of quantum mechanical uncertainties in the I_x and I_y components.

At equilibrium, the different energy states are unequally populated because lower energy orientations of the magnetic dipole vector are more probable. The relative population of a state is given by the Boltzmann distribution,

$$\begin{aligned}\frac{N_m}{N} &= \exp\left(\frac{-E_m}{k_B T}\right) \Bigg/ \sum_{m=-I}^{I} \exp\left(\frac{-E_m}{k_B T}\right) \\ &= \exp\left(\frac{m\hbar\gamma B_0}{k_B T}\right) \Bigg/ \sum_{m=-I}^{I} \exp\left(\frac{m\hbar\gamma B_0}{k_B T}\right) \\ &\approx \left(1 + \frac{m\hbar\gamma B_0}{k_B T}\right) \Bigg/ \sum_{m=-I}^{I} \left(1 + \frac{m\hbar\gamma B_0}{k_B T}\right) \\ &\approx \frac{1}{2I+1}\left(1 + \frac{m\hbar\gamma B_0}{k_B T}\right), \end{aligned} \qquad [1.6]$$

in which N_m is the number of nuclei in the mth state and N is the total number of spins, T is the absolute temperature, and k_B is the Boltzmann constant. The last two lines of [1.6] are obtained by expanding the exponential functions to first order using Taylor series, because at temperatures relevant for solution NMR spectroscopy, $m\hbar\gamma B_0/k_B T \ll 1$. The populations of the states depend both on the nucleus type and on the applied field strength. As the external field strength increases, the energy differences between the nuclear spin energy levels become larger and the population differences between the states increase. Of course, polarization of the spin system to generate a population difference between spin states does not occur instantaneously upon application of the magnetic field; instead, the polarization, or magnetization, develops with a characteristic rate constant, called the spin–lattice relaxation rate constant (see Chapter 5).

The bulk magnetic moment, **M**, and the bulk angular momentum, **J**, of a macroscopic sample are given by the vector sum of the corresponding quantities for individual nuclei, $\boldsymbol{\mu}$ and **I**. At thermal equilibrium, the transverse components (e.g., the x- or y-components) of $\boldsymbol{\mu}$ and **I** for different nuclei in the sample are uncorrelated and sum to zero. The small population differences between energy levels give rise to a bulk magnetization of the sample parallel (longitudinal) to the static magnetic field, $\mathbf{M} = M_0\mathbf{k}$, in which **k** is the unit vector in the z-direction.

Using [1.2], [1.3], and [1.6], M_0 is given by

$$\begin{aligned} M_0 &= \gamma\hbar \sum_{m=-I}^{I} mN_m \\ &= N\gamma\hbar \sum_{m=-I}^{I} m \exp(m\gamma\hbar B_0/k_B T) \Big/ \sum_{m=-I}^{I} \exp(m\gamma\hbar B_0/k_B T) \\ &\approx N\gamma\hbar \sum_{m=-I}^{I} m(1 + m\gamma\hbar B_0/k_B T) \Big/ \sum_{m=-I}^{I} (1 + m\gamma\hbar B_0/k_B T) \\ &\approx \left[N\gamma^2\hbar^2 B_0/k_B T(2I+1)\right] \sum_{m=-I}^{I} m^2 \\ &\approx N\gamma^2\hbar^2 B_0 I(I+1)/(3k_B T). \end{aligned} \quad [1.7]$$

By analogy with other areas of spectroscopy, transitions between Zeeman levels can be stimulated by applied electromagnetic radiation. The selection rule governing magnetic dipole transitions is $\Delta m = \pm 1$. Thus, the photon energy, ΔE, required to excite a transition between the m and $m+1$ Zeeman states is

$$\Delta E = \hbar\gamma B_0, \quad [1.8]$$

which is seen to be directly proportional to the magnitude of the static magnetic field. By Planck's Law, the frequency of the required electromagnetic radiation is given by

$$\omega = \Delta E/\hbar = \gamma B_0, \qquad \nu = \omega/2\pi = \gamma B_0/2\pi, \quad [1.9]$$

in units of s^{-1} or Hertz, respectively. The sensitivity of NMR spectroscopy depends upon the population differences between Zeeman states. The population difference is only on the order of 1 in 10^5 for ^1H spins in an 11.7-T magnetic field. As a result, NMR is an insensitive spectroscopic technique compared to techniques such as visible or ultraviolet spectroscopy. This simple observation explains much of the impetus to construct more powerful magnets for use in NMR spectroscopy.

For the most part, this text is concerned with the NMR spectroscopy of spin $I = 1/2$ (spin-1/2) nuclei. For an isolated spin, only two nuclear spin states exist and two energy levels separated by $\Delta E = \hbar\gamma B_0$ are obtained by application of an external magnetic field. A single Zeeman

transition between the energy levels exists. The spin state with $m = +1/2$ is referred to as the α state, and the state with $m = -1/2$ is referred to as the β state. If γ is positive (negative), then the α state has lower (higher) energy compared to the β state.

1.2 The Bloch Equations

Bloch formulated a simple semiclassical vector model to describe the behavior of a sample of noninteracting spin-1/2 nuclei in a static magnetic field (*11*). The Bloch model is outlined briefly in this section; many of the concepts and terminology introduced persist throughout the text.

The evolution of the bulk magnetic moment, $\mathbf{M}(t)$, represented as a vector quantity, is central to the Bloch formalism. In the presence of a magnetic field, which may include components in addition to the static field, $\mathbf{M}(t)$ experiences a torque that is equal to the time derivative of the angular momentum,

$$\frac{d\mathbf{J}(t)}{dt} = \mathbf{M}(t) \times \mathbf{B}(t). \qquad [1.10]$$

Multiplying both sides by γ yields

$$\frac{d\mathbf{M}(t)}{dt} = \mathbf{M}(t) \times \gamma\mathbf{B}(t). \qquad [1.11]$$

The physical significance of this equation can be seen by using a frame of reference rotating with respect to the fixed laboratory axes. The angular velocity of the rotating axes is represented by the vector $\boldsymbol{\omega}$. Without loss of generality, the two coordinate systems are assumed to be superposed initially. Vectors are represented identically in the two coordinate systems; however, time differentials are represented differently in the two coordinate systems. The equations of motion of $\mathbf{M}(t)$ in the laboratory and rotating frames are related by (*12*)

$$\begin{aligned}\left[\frac{d\mathbf{M}(t)}{dt}\right]_{\text{rot}} &= \left[\frac{d\mathbf{M}(t)}{dt}\right]_{\text{lab}} + \mathbf{M}(t) \times \boldsymbol{\omega} \\ &= \mathbf{M}(t) \times [\gamma\mathbf{B}(t) + \boldsymbol{\omega}]. \end{aligned} \qquad [1.12]$$

The equation of motion for the magnetization in the rotating frame has the same form as in the laboratory frame, provided that the field $\mathbf{B}(t)$ is replaced by an effective field, $\mathbf{B}_{\text{eff}}$, given by

$$\mathbf{B}_{\text{eff}} = \mathbf{B}(t) + \boldsymbol{\omega}/\gamma. \qquad [1.13]$$

For the choice $\boldsymbol{\omega} = -\gamma\mathbf{B}(t)$, the effective field is zero, so that $\mathbf{M}(t)$ is time independent in the rotating frame. Consequently, as seen from the laboratory frame, $\mathbf{M}(t)$ precesses around $\mathbf{B}(t)$ with a frequency $\boldsymbol{\omega} = -\gamma B$. For a static field of strength B_0, the precessional frequency, or the *Larmor frequency*, is given by

$$\omega_0 = -\gamma B_0. \qquad [1.14]$$

Thus, in the absence of other magnetic fields, the bulk magnetization precesses at the Larmor frequency around the main static field axis (defined as the z-direction). As discussed by Levitt (*13*), the Larmor frequency has different signs for spins with positive or negative gyromagnetic ratios, e.g., ^{1}H and ^{15}N, and this fact historically has caused confusion in correctly determining the absolute sign of NMR parameters. The magnitude of the precessional frequency is identical to the frequency of electromagnetic radiation required to excite transitions between Zeeman levels [1.9]. This identity is the reason that, within limits, a classical description of NMR spectroscopy is valid for systems of isolated spin-1/2 nuclei.

Before proceeding further, the nomenclature used to refer to the strength of a magnetic field needs to be clarified. In NMR spectroscopy, the magnetic field strength B normally appears in the equation $\omega = -\gamma B$ that defines the precessional frequency of the nuclear magnetic moment. Conventionally, γB is referred to as the magnetic field strength measured in frequency units. Strictly speaking, the strength of the magnetic field is B, measured in Gauss or Tesla ($10^4\,\text{G} = 1\,\text{T}$); therefore, denoting γB as the magnetic field strength is incorrect (and has the obvious disadvantage of depending on the type of nucleus considered). That said, however, measuring magnetic field strength in frequency units (s^{-1} or Hertz) is very convenient in many cases. Consequently, throughout this text, both terms, γB and B, will be used to denote field strength in appropriate units. For example, common usage refers to NMR spectrometers by the proton Larmor frequency of the magnet; thus, a spectrometer with an 11.7-T magnet is termed a 500-MHz spectrometer, and a spectrometer with a 21.2-T magnet is termed a 900-MHz spectrometer.

Precession of the bulk magnetic moment about the static magnetic field constitutes a time-varying magnetic field. According to Faraday's law of induction, a time-varying magnetic field produces an induced electromotive force in a coil of appropriate geometry located in the vicinity of the bulk sample (*14*, *15*). Equation [1.11] suggests that precession of the bulk nuclear magnetization can be detected by such a mechanism. However, at thermal equilibrium, the bulk magnetization vector is collinear with the static field and no signal is produced in the coil. The key to producing an NMR signal is to disturb this equilibrium state. This text has as its subject *pulsed* NMR experiments in which a short burst of radiofrequency (rf) electromagnetic radiation, typically of the order of several microseconds in duration, displaces the bulk magnetization from equilibrium. Such rf bursts are referred to as pulses. After the rf field is turned off, the bulk magnetization vector, $\mathbf{M}(t)$, will not, in general, be parallel to the static field. Consequently, the bulk magnetization will precess around the static field with an angular frequency $\omega_0 = -\gamma B_0$ and will generate a detectable signal in the coil.

The magnetic component of an rf field that is linearly polarized along the x-axis of the laboratory frame is written as

$$\begin{aligned}\mathbf{B}_{\mathrm{rf}}(t) &= 2B_1 \cos(\omega_{\mathrm{rf}} t + \phi)\mathbf{i} \\ &= B_1\{\cos(\omega_{\mathrm{rf}} t + \phi)\mathbf{i} + \sin(\omega_{\mathrm{rf}} t + \phi)\mathbf{j}\} \\ &\quad + B_1\{\cos(\omega_{\mathrm{rf}} t + \phi)\mathbf{i} - \sin(\omega_{\mathrm{rf}} t + \phi)\mathbf{j}\},\end{aligned} \qquad [1.15]$$

where B_1 is the amplitude of the applied field, ω_{rf} is the angular frequency of the rf field, often called the *transmitter* or *carrier frequency*, ϕ is the phase of the field, and $\mathbf{i}$ and $\mathbf{j}$ are unit vectors defining the x- and y-axes, respectively. In the present context, the amplitude and phase of the rf field are assumed to be constant; time-varying amplitude- or phase-modulated rf fields are considered in Section 3.4. In the second equality in [1.15], the rf field is decomposed into two circularly polarized fields rotating in opposite directions about the z-axis. Only the field rotating in the same sense as the magnetic moment interacts significantly with the magnetic moment; the counter-rotating, nonresonant field influences the spins to order $(B_1/2B_0)^2$, which is normally a very small number known as the Bloch-Siegert shift (but see Section 3.4.1). Thus, the nonresonant term can be ignored and the rf field is written simply as

$$\mathbf{B}_{\mathrm{rf}}(t) = B_1\{\cos(\omega_{\mathrm{rf}} t + \phi)\mathbf{i} + \sin(\omega_{\mathrm{rf}} t + \phi)\mathbf{j}\}. \qquad [1.16]$$

In the case of a time-dependent field such as this, the solution to [1.11] can be found by moving to a rotating frame, which makes the perturbing field time independent. This is referred to as the *rotating frame transformation*. The new frame is chosen to rotate at angular frequency ω_{rf} about the z-axis. The equation of motion for the magnetization in the rotating frame, $\mathbf{M}^r(t)$, is given by

$$\frac{d\mathbf{M}^r(t)}{dt} = \mathbf{M}^r(t) \times \gamma \mathbf{B}^r(t), \qquad [1.17]$$

in which the effective field, $\mathbf{B}^r$, in the rotating frame is given by

$$\mathbf{B}^r = B_1 \cos\phi \mathbf{i}^r + B_1 \sin\phi \mathbf{j}^r + \Delta B_0 \mathbf{k}^r; \qquad [1.18]$$

here ΔB_0 is known as the reduced static field and is equivalent to the z-component of the effective field,

$$\Delta B_0 = -\Omega/\gamma, \qquad [1.19]$$

and $\Omega = -\gamma B_0 - \omega_{rf} = \omega_0 - \omega_{rf}$ is known as the *offset*, and $\mathbf{i}^r$, $\mathbf{j}^r$, and $\mathbf{k}^r$ are unit vectors in the rotating frame. Equation [1.17] differs from [1.12] only because the quantities on both sides of the equality have been expressed in the rotating frame. The rf field is described by the amplitude B_1 and the phase ϕ. In accordance with Ernst et al. (*16*), the phase angle has been defined such that for an rf field of fixed phase x, $B_x = B_1$ and $B_y = 0$. The magnitude of the effective field is given by

$$B^r = \sqrt{(B_1)^2 + (\Delta B_0)^2} = B_1 / \sin\theta \qquad [1.20]$$

and the angle θ through which the effective field is tilted with respect to the z-axis is defined by

$$\tan\theta = \frac{B_1}{\Delta B_0} = \frac{-\gamma B_1}{\Omega} = \frac{\omega_1}{\Omega}, \qquad [1.21]$$

in which $\omega_1 = -\gamma B_1$.The direction of the effective field, as defined by θ and ϕ, depends on the strength of the rf field, $\mathbf{B}_{rf}(t)$, the difference between the transmitter and Larmor frequencies, and the phase of the rf field in the laboratory frame, as illustrated in Fig. 1.2. Frequently, $\mathbf{B}_{rf}(t)$ is referred to directly as the "B_1 field." In the rotating frame, upon application of the B_1 field, $\mathbf{M}^r(t)$ precesses around the effective field $\mathbf{B}^r$

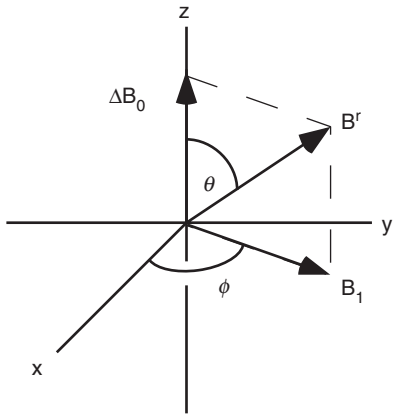

FIGURE 1.2 Orientations of $\Delta\mathbf{B}_0$, $\mathbf{B}_1$, and $\mathbf{B}^r$ in the rotating reference frame. Angles θ and ϕ are defined by [1.21] and [1.18].

with an angular frequency ω^r,

$$\omega^r = -\gamma B^r. \qquad [1.22]$$

If the rf field is turned on for a time period τ_p, called the *pulse length*, then the effective rotation angle α (or flip angle) is given by

$$\alpha = \omega^r \tau_p = -\gamma B^r \tau_p = -\gamma B_1 \tau_p / \sin\theta = \omega_1 \tau_p / \sin\theta. \qquad [1.23]$$

If the transmitter frequency, ω_{rf}, is equal to ω_0, then the irradiation is said to be applied *on-resonance*. In the on-resonance case, the offset term, Ω, equals zero, $B^r = B_1$, and the effective field is collinear with the B_1 field in the rotating frame. These results have an important implication: *the influence of the main static magnetic field*, $\mathbf{B}_0$, *has been removed*. The bulk magnetization $\mathbf{M}^r(t)$ precesses around the axis defined by the B_1 field, with frequency $\omega^r = -\gamma B^r = -\gamma B_1 = \omega_1$. Precession of the magnetization about the effective field in the rotating reference frame is illustrated in Fig. 1.3. As general practice in this text, the rotating frame will not be indicated explicitly, and unless otherwise stated, the rotating frame of reference will be assumed [i.e., $\mathbf{M}(t)$ will be written instead of $\mathbf{M}^r(t)$].

Following an rf pulse, the bulk magnetization precesses about the static magnetic field with a Larmor frequency ω_0. As described previously, following an initial pulse, the magnetization would continue

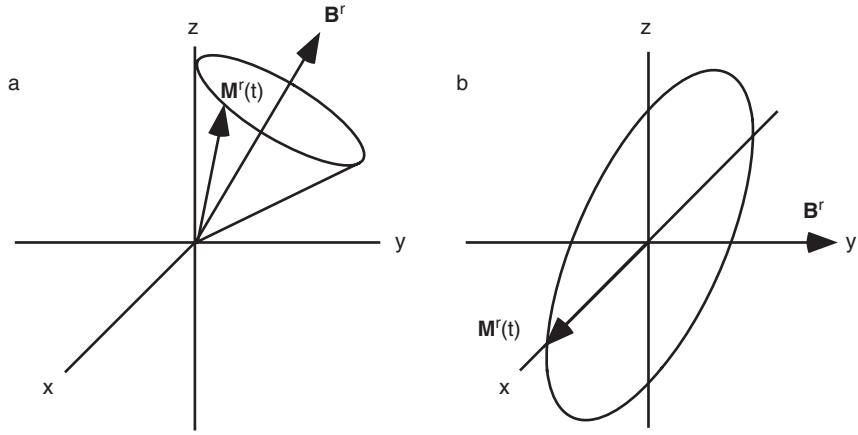

FIGURE 1.3 Effect of applied rf field. (a) In the presence of an applied rf field with y-phase, the effective field, $\mathbf{B}^r$ is in the y–z plane in the rotating reference frame, and the magnetization vector, $\mathbf{M}^r(t)$, precesses around $\mathbf{B}^r$. (b) If the rf field is applied on-resonance, then $\mathbf{B}^r$ is oriented along the y-axis, and $\mathbf{M}^r(t)$ rotates in the x–z plane orthogonal to $\mathbf{B}^r$.

to evolve freely in the transverse plane forever. This, of course, is not the case because eventually thermal equilibrium must be re-established. Bloch defined two processes to account for the observed decay of the NMR signal (*11*). These two relaxation processes are responsible for the return of the bulk magnetization to the equilibrium state following some perturbation to the nuclear spin system. The first relaxation mechanism accounts for the return of the population difference across the Zeeman transition back to the Boltzmann equilibrium distribution, and is known as longitudinal, or spin–lattice, relaxation. Bloch assumed that spin–lattice relaxation is characterized by the first-order rate expression,

$$\frac{dM_z(t)}{dt} = R_1[M_0 - M_z(t)], \qquad [1.24]$$

such that

$$M_z(t) = M_0 - [M_0 - M_z(0)] \exp(-R_1 t), \qquad [1.25]$$

in which R_1 is the spin–lattice relaxation rate constant (the spin–lattice relaxation time constant, $T_1 = 1/R_1$, is often encountered), and $M_z(0)$

is the value of the component of the magnetization along the z-axis at $t=0$. As shown, the z-component, or longitudinal, magnetization returns to thermal equilibrium in an exponential fashion. A second relaxation process was introduced to account for the decay of the transverse magnetization in the x–y plane following a pulse. Transverse, or spin–spin, relaxation also is characterized by a first-order rate expression,

$$\begin{aligned}\frac{dM_x(t)}{dt} &= -R_2 M_x(t),\\ \frac{dM_y(t)}{dt} &= -R_2 M_y(t),\end{aligned} \qquad [1.26]$$

and

$$\begin{aligned}M_x(t) &= M_x(0)\exp(-R_2 t),\\ M_y(t) &= M_y(0)\exp(-R_2 t),\end{aligned} \qquad [1.27]$$

in which R_2 is the spin–spin relaxation rate constant (the spin–spin relaxation time constant is $T_2 = 1/R_2$) and $M_x(0)$ and $M_y(0)$ are the values of the transverse magnetization at $t=0$. The introduction of the concept of relaxation here is simply to assist in the initial description of the NMR phenomenon, and more detailed treatments of relaxation theory and processes will be presented in Chapter 5.

Combining [1.11], [1.24], and [1.26] yields the famous Bloch equations in the laboratory reference frame:

$$\begin{aligned}\frac{dM_x(t)}{dt} &= \gamma\Big[\mathbf{M}(t)\times\mathbf{B}(t)\Big]_x - R_2 M_x(t)\\ &= \gamma\Big[M_y(t)B_z(t) - M_z(t)B_y(t)\Big] - R_2 M_x(t),\\ \frac{dM_y(t)}{dt} &= \gamma\Big[\mathbf{M}(t)\times\mathbf{B}(t)\Big]_y - R_2 M_y(t)\\ &= \gamma\Big[M_z(t)B_x(t) - M_x(t)B_z(t)\Big] - R_2 M_y(t),\\ \frac{dM_z(t)}{dt} &= \gamma\Big[\mathbf{M}(t)\times\mathbf{B}(t)\Big]_z - R_1\Big[M_z(t) - M_0\Big]\\ &= \gamma\Big[M_x(t)B_y(t) - M_y(t)B_x(t)\Big] - R_1\Big[M_z(t) - M_0\Big],\end{aligned} \qquad [1.28]$$

describing the evolution of magnetization in a magnetic field. In the rotating reference frame, the Bloch equations are given by

$$\begin{aligned}
\frac{dM_x(t)}{dt} &= -\Omega M_y(t) + \omega_1 \sin\phi M_z(t) - R_2 M_x(t), \\
\frac{dM_y(t)}{dt} &= \Omega M_x(t) - \omega_1 \cos\phi M_z(t) - R_2 M_y(t), \\
\frac{dM_z(t)}{dt} &= \omega_1\Big[-\sin\phi M_x(t) + \cos\phi M_y(t)\Big] - R_1\Big[M_z(t) - M_0\Big].
\end{aligned} \tag{1.29}$$

These equations can be written in a convenient matrix form as

$$\frac{d\mathbf{M}(t)}{dt} = \begin{bmatrix} -R_2 & -\Omega & \omega_1 \sin\phi \\ \Omega & -R_2 & -\omega_1 \cos\phi \\ -\omega_1 \sin\phi & \omega_1 \cos\phi & -R_1 \end{bmatrix} \mathbf{M}(t) + R_1 M_0 \begin{bmatrix} 0 \\ 0 \\ 1 \end{bmatrix}, \tag{1.30}$$

in which

$$\mathbf{M}(t) = \begin{bmatrix} M_x(t) \\ M_y(t) \\ M_z(t) \end{bmatrix}. \tag{1.31}$$

In the absence of an applied rf field, $\omega_1 = 0$ and the Bloch equations become

$$\begin{aligned}
\frac{dM_x(t)}{dt} &= -\Omega M_y(t) - R_2 M_x(t), \\
\frac{dM_y(t)}{dt} &= \Omega M_x(t) - R_2 M_y(t), \\
\frac{dM_z(t)}{dt} &= -R_1[M_z(t) - M_0].
\end{aligned} \tag{1.32}$$

Evolution in the absence of an applied rf field is referred to as *free precession*.

In a common experimental situation in pulsed NMR spectroscopy, the B_1 field is applied for a time $\tau_p \ll 1/R_2$ and $1/R_1$, and the Bloch equations simplify to

$$\frac{d\mathbf{M}(t)}{dt} = \begin{bmatrix} 0 & -\Omega & \omega_1 \sin\phi \\ \Omega & 0 & -\omega_1 \cos\phi \\ -\omega_1 \sin\phi & \omega_1 \cos\phi & 0 \end{bmatrix} \mathbf{M}(t). \tag{1.33}$$

If neither B_1 nor ϕ is time dependent, then the solution to [1.33] can be represented as a series of rotations (*16, 17*):

$$\mathbf{M}(\tau_p) = \mathbf{R}_z(\phi)\mathbf{R}_y(\theta)\mathbf{R}_z(\alpha)\mathbf{R}_y(-\theta)\mathbf{R}_z(-\phi)\mathbf{M}(0), \qquad [1.34]$$

in which the rotation matrices are

$$\mathbf{R}_x(\beta) = \begin{bmatrix} 1 & 0 & 0 \\ 0 & \cos\beta & -\sin\beta \\ 0 & \sin\beta & \cos\beta \end{bmatrix},$$
$$\mathbf{R}_y(\beta) = \begin{bmatrix} \cos\beta & 0 & \sin\beta \\ 0 & 1 & 0 \\ -\sin\beta & 0 & \cos\beta \end{bmatrix}, \qquad [1.35]$$
$$\mathbf{R}_z(\beta) = \begin{bmatrix} \cos\beta & -\sin\beta & 0 \\ \sin\beta & \cos\beta & 0 \\ 0 & 0 & 1 \end{bmatrix}.$$

In [1.35], the notation $\mathbf{R}_x(\beta)$ designates a right-handed rotation of angle β about the axis x. A positive rotation is counterclockwise when viewed down the axis x toward the origin, or clockwise when viewed from the origin along x. The rotation matrices and [1.34] will be used frequently to calculate the effect of rf pulses on isolated spins. For example, the effect of an x-phase ($\phi = 0$) pulse is described by

$$\mathbf{M}(\tau_p) = \begin{bmatrix} \cos^2\theta\cos\alpha + \sin^2\theta & -\cos\theta\sin\alpha & \cos\theta\sin\theta(1-\cos\alpha) \\ \cos\theta\sin\alpha & \cos\alpha & -\sin\theta\sin\alpha \\ \cos\theta\sin\theta(1-\cos\alpha) & \sin\theta\sin\alpha & \sin^2\theta\cos\alpha + \cos^2\theta \end{bmatrix}\mathbf{M}(0). \qquad [1.36]$$

The effective rotation angle, α_{12}, and rotation axis, $\mathbf{n}_{12}$, that result from consecutive pulses with rotation angles α_1 and α_2, respectively, and rotation axes, $\mathbf{n}_1$ and $\mathbf{n}_2$, respectively, can be determined using the quarternion formalism to be (*18*)

$$\cos\left(\frac{\alpha_{12}}{2}\right) = \cos\left(\frac{\alpha_1}{2}\right)\cos\left(\frac{\alpha_2}{2}\right) - \sin\left(\frac{\alpha_1}{2}\right)\sin\left(\frac{\alpha_2}{2}\right)\mathbf{n}_1 \cdot \mathbf{n}_2,$$
$$\sin\left(\frac{\alpha_{12}}{2}\right)\mathbf{n}_{12} = \sin\left(\frac{\alpha_1}{2}\right)\cos\left(\frac{\alpha_2}{2}\right)\mathbf{n}_1 + \cos\left(\frac{\alpha_1}{2}\right)\sin\left(\frac{\alpha_2}{2}\right)\mathbf{n}_2$$
$$- \sin\left(\frac{\alpha_1}{2}\right)\sin\left(\frac{\alpha_2}{2}\right)\mathbf{n}_1 \times \mathbf{n}_2. \qquad [1.37]$$

These equations can be applied iteratively to generate expressions for three or more rotations and are particularly useful in determining the effective rotations produced by composite pulses (see Section 3.4.2).

1.3 The One-Pulse NMR Experiment

Experimental aspects of NMR spectroscopy are described in detail in Chapter 3. In this section, a brief overview of a simple NMR experiment is presented. In the Bloch model, the maximum NMR signal is detected when the bulk magnetic moment is perpendicular (transverse) to the static magnetic field. As noted previously, an rf pulse causes $\mathbf{M}(t)$ to precess about an axis defined by the direction of the effective magnetic field in the rotating frame; therefore, the properties of an rf pulse that cause rotation of $\mathbf{M}(t)$ from the z-axis through an angle of 90° are particularly important in pulsed NMR spectroscopy.

An ideal one-pulse experiment that achieves a 90° rotation of $\mathbf{M}(t)$ will be considered. An rf pulse of duration τ_p, strength B_1, and tilt angle $\theta = \pi/2$ is applied to the equilibrium magnetization state. If the rf pulse is applied along the y-axis of the rotating frame (setting $\phi = \pi/2$ in [1.18]), then the magnetization following the pulse is given by (see [1.34])

$$\mathbf{M}(\tau_p) = \mathbf{R}_y(\alpha)\mathbf{M}_0 = \mathbf{i}M_0 \sin\alpha + \mathbf{k}M_0 \cos\alpha = \begin{bmatrix} M_0 \sin\alpha \\ 0 \\ M_0 \cos\alpha \end{bmatrix}, \qquad [1.38]$$

where M_0 is the magnitude of the equilibrium magnetization and α is the rotation angle. The maximum transverse magnetization is generated for a rotation angle of 90°. The rf pulse used to achieve this state is conventionally called a *90°* or *(π/2) pulse*. A 90° pulse equalizes the populations of the α and β spin states. In contrast, a *180°* (or π) *pulse* generates no transverse magnetization. Instead, the bulk magnetization is inverted from its original state to yield $\mathbf{M}(\tau_p) = -M_0\mathbf{k}$. In the Bloch vector model, the bulk magnetization following a 180° pulse is aligned along the $-z$-axis. This corresponds to a population inversion between the α and β states, such that the β state now possesses excess (deficient) population of nuclei for positive (negative) γ. The populations of the Zeeman states and the net magnetization vectors following on-resonance pulses are illustrated in Fig. 1.4.

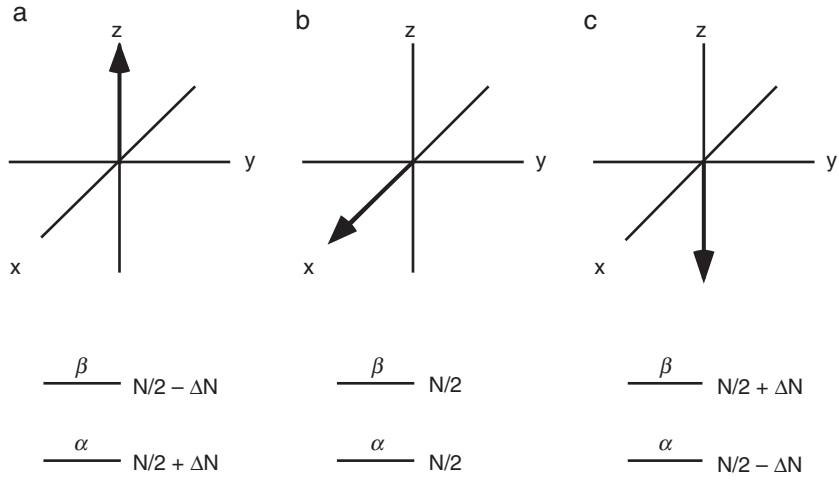

FIGURE 1.4 On-resonance pulses. Shown are the magnetization vectors and spin states α and β (a) for thermal equilibrium, (b) following a 90° pulse with y-phase, and (c) following a 180° pulse. The populations of each spin state are indicated for positive γ. The total number of spins is N and $\Delta N = N\hbar\gamma B_0/(4k_B T)$.

Following the pulse, the magnetization precessing during the so-called *acquisition period, t*, generates the signal that is recorded by the NMR spectrometer. The signal is referred to as a *free induction decay* (FID). The free-precession Bloch equations in the rotating frame [1.32] show that the free induction decay can be described in terms of two components,

$$\begin{aligned} M_x(t) &= M_0 \sin\alpha \cos(\Omega t) \exp(-R_2 t), \\ M_y(t) &= M_0 \sin\alpha \sin(\Omega t) \exp(-R_2 t), \end{aligned} \qquad [1.39]$$

which can be combined in complex notation as

$$M^+(t) = M_x(t) + iM_y(t) = M_0 \sin\alpha \exp(i\Omega t - R_2 t). \qquad [1.40]$$

As a consequence of relaxation, the components of the bulk magnetization vector precessing in the transverse plane following an rf pulse are damped by the exponential factor $\exp(-R_2 t)$. In practice, both parts of the complex signal are detected simultaneously by the NMR spectrometer as $s^+(t) = \lambda M^+(t)$, with λ being an experimental constant

of proportionality. The complex time-domain signal is Fourier transformed to produce the complex frequency-domain spectrum,

$$S(\omega) = \int_0^\infty s^+(t)\, \exp(-i\omega t)\, dt$$
$$= v(\omega) + iu(\omega), \qquad [1.41]$$

in which

$$v(\omega) = \lambda M_0 \frac{R_2}{R_2^2 + (\Omega - \omega)^2}, \qquad [1.42]$$

$$u(\omega) = \lambda M_0 \frac{\Omega - \omega}{R_2^2 + (\Omega - \omega)^2}. \qquad [1.43]$$

The function $v(\omega)$ represents a signal with an absorptive Lorentzian lineshape and the function $u(\omega)$ represents a signal with the corresponding dispersive Lorentzian lineshape. The real part of the complex spectrum, $v(\omega)$, normally is displayed as the NMR spectrum. This simple one-pulse NMR experiment is illustrated schematically in Fig. 1.5.

1.4 Linewidth

The phenomenological linewidth is defined as the full-width at half-height (FWHH) of the resonance lineshape and is a primary factor affecting both resolution and signal-to-noise ratio of NMR spectra. The homogeneous linewidth is determined by intrinsic molecular properties while the inhomogeneous linewidth contains contributions from instrumental imperfections, such as static magnetic field inhomogeneity or thermal gradients within the sample. For a Lorentzian lineshape [1.42], the homogeneous linewidth is given by $\Delta\nu_{\mathrm{FWHH}} = R_2/\pi$ in Hertz (or $\Delta\omega_{\mathrm{FWHH}} = 2R_2$ in angular units, s^{-1}) and the inhomogeneous linewidth is $\Delta\nu_{\mathrm{FWHH}} = R_2^*/\pi$, in which $R_2^* = R_2 + R_{\mathrm{inhom}}$, and R_{inhom} represents the broadening of the resonance signal due to instrumental imperfections. In modern NMR spectrometers R_{inhom}/π is on the order of 1 Hz (in the absence of significant temperature gradients in the sample). As will be discussed in detail in Chapter 5, values of R_2 (and hence homogeneous linewidths) are proportional to the overall rotational correlation time of the protein, τ_c, and thus depend on molecular mass and shape of the molecule, with larger molecules having larger

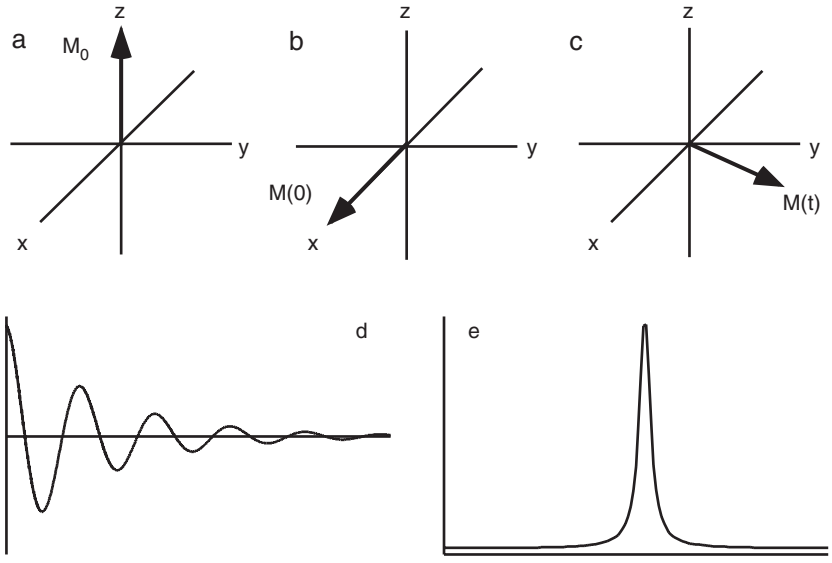

FIGURE 1.5 One-pulse NMR experiment. Shown are (a) the orientation along the z-axis of the net magnetization at equilibrium, (b) the orientation along the x-axis of the net magnetization at the start of acquisition following a 90° pulse with y-phase, (c) the precessing magnetization in the x–y plane, (d) the FID recorded for the precessing magnetization during the acquisition period, and (e) the real component of the complex frequency domain NMR spectrum obtained by Fourier transformation of the FID.

linewidths. As discussed in Section 6.1, observed linewidths significantly larger than expected based on the molecular mass of the protein imply that aggregation is increasing the apparent rotational correlation time or that chemical exchange effects (Section 5.6) contribute significantly to the linewidth.

Given theoretical or experimental estimates of τ_c, the theoretical equations presented in Chapters 5 and 7 can be used to calculate approximate values of resonance linewidths. The resulting curves are shown in Fig. 1.6. The principal uncertainties in the calculation are due to the following factors: (*i*) anisotropic rotational diffusion of non-spherical molecules, (*ii*) differential contributions from internal motions (particularly in loops or for side chains), (*iii*) cross-correlation effects, (*iv*) dipolar interactions with nearby ^{1}H spins (which depend on detailed structures of the proteins), and (*v*) incomplete knowledge of fundamental parameters (such as chemical shift anisotropies).

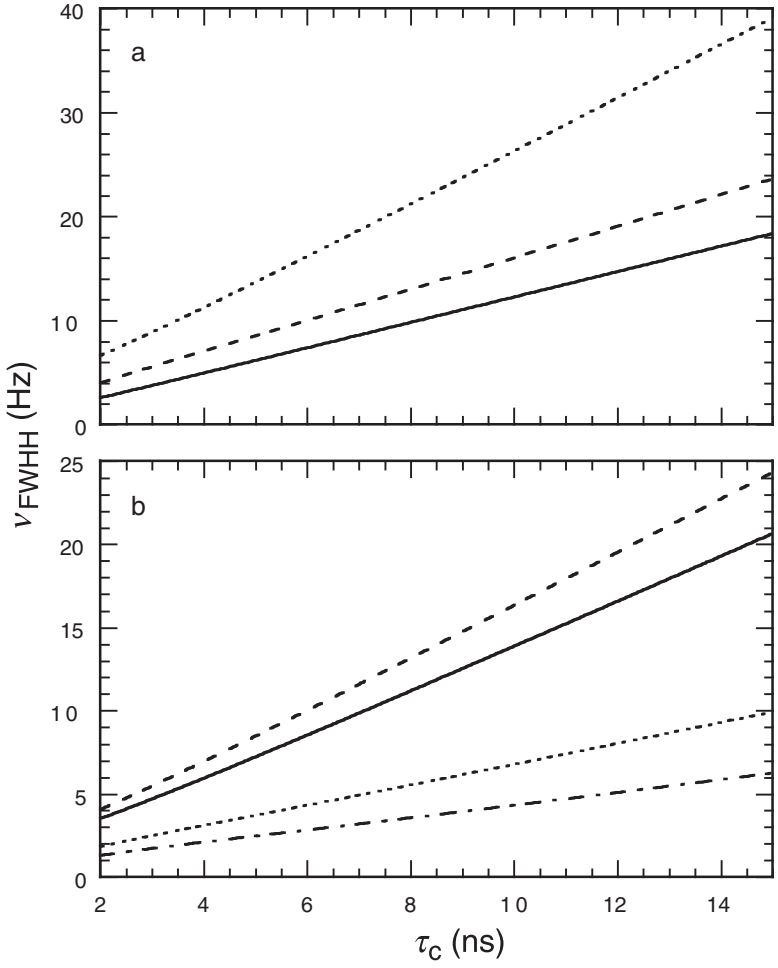

FIGURE 1.6 Resonance linewidths. Protein resonance linewidths are shown as a function of rotational correlation time. (a) Linewidths for ^{1}H spins (solid), ^{1}H spins covalently bonded to ^{13}C (dotted), and ^{1}H spins covalently bonded to ^{15}N nuclei (dashed). (b) Heteronuclear linewidths for proton-decoupled ^{13}C (solid), proton-coupled ^{13}C (dashed), proton-decoupled ^{15}N (dash-dot), and proton-coupled ^{15}N spins (dotted). Calculations included dipolar relaxation of all spins, and CSA relaxation of ^{15}N spins. For ^{1}H–^{1}H dipolar interactions, $\sum_j r_{ij}^{-6} = 0.027\,\text{Å}^{-6}$ (*49*).

The correlation time for Brownian rotational diffusion can be measured experimentally by using time-resolved fluorescence spectroscopy, light scattering, and NMR spin relaxation spectroscopy, or can be calculated by using a variety of hydrodynamic theories (that unfortunately require detailed information on the shape of the molecule) (*19*). In the absence of more accurate information, the simplest theoretical approach for approximately spherical globular proteins calculates the isotropic rotational correlation time from Stokes' law:

$$\tau_c = 4\pi\eta_w r_H^3/(3k_B T), \qquad [1.44]$$

in which η_w is the viscosity of the solvent, r_H is the effective hydrodynamic radius of the protein, k_B is the Boltzmann constant, and T is the temperature. The hydrodynamic radius can be very roughly estimated from the molecular mass of the protein, M_r, by assuming that the specific volume of the protein is $\overline{V} = 0.73\,\text{cm}^3/\text{g}$ and that a hydration layer of $r_w = 1.6$ to $3.2\,\text{Å}$ (corresponding to one-half to one hydration shell) surrounds the protein (*20*):

$$r_H = \left[3\overline{V}M_r/(4\pi N_A)\right]^{1/3} + r_w, \qquad [1.45]$$

in which N_A is Avogadro's number. Rotational correlation times in D_2O solution are approximately 25% greater than in H_2O solution because of the larger viscosity of D_2O.

The small protein ubiquitin is used as an example throughout this text. The protein sequence consists of 76 amino acid residues and $M_r = 8400$. For ubiquitin, $r_H = 16.5\,\text{Å}$ is calculated from [1.45], and $\tau_c = 3.8\,\text{ns}$ at $300\,\text{K}$ is calculated from [1.44]. This estimate can be compared with a value of 4.1 ns determined from NMR spectroscopy (*21*). In light of the uncertainties, the results presented in Fig. 1.6 should be regarded as approximate guidelines. For example, ^1H (in an unlabeled sample), $^{13}C^{\alpha}$, and ^{15}N linewidths are ~6–9, ~7, and ~3 Hz, respectively, for ubiquitin. These values are consistent with values of 5, 6, and 2 Hz determined from Fig. 1.6.

1.5 Chemical Shift

A general feature of NMR spectroscopy is that the observed resonance frequencies depend on the local environments of individual nuclei and differ slightly from the frequencies predicted by [1.14]. The differences in resonance frequencies are referred to as *chemical shifts*

and offer the possibility of distinguishing between otherwise identical nuclei in different chemical environments.

The phenomenon of chemical shift arises because motions of electrons induced by the external magnetic field generate secondary magnetic fields. The net magnetic field at the location of a specific nucleus depends upon the static magnetic field and the local secondary fields. The effect of the secondary fields is called *nuclear shielding* and can augment or diminish the effect of the main field. In general, the electronic charge distribution in a molecule is anisotropic and the effects of shielding on a particular nucleus are described by the second-rank nuclear shielding tensor, represented by a 3×3 matrix. In the principal coordinate system of the shielding tensor, the matrix representing the tensor is diagonal, with principal components σ_{11}, σ_{22}, and σ_{33}. If the molecule is oriented such that the kth principal axis is oriented along the z-axis of the static field, then the net magnetic field at the nucleus is given by

$$B = (1 - \sigma_{kk})B_0. \qquad [1.46]$$

In isotropic liquid solution, collisions lead to rapid reorientation of the molecule and, consequently, of the shielding tensor. Under these circumstances, the effects of shielding on a particular nucleus can be accounted for by modifying [1.14] as

$$\omega = -\gamma(1 - \sigma)B_0, \qquad [1.47]$$

in which σ is the average, isotropic, shielding constant for the nucleus:

$$\sigma = (\sigma_{11} + \sigma_{22} + \sigma_{33})/3. \qquad [1.48]$$

The chemical shift anisotropy (CSA) is defined as

$$\Delta\sigma = \sigma_{11} - (\sigma_{22} + \sigma_{33})/2, \qquad [1.49]$$

and the asymmetry of the tensor is defined as

$$\eta = \frac{3(\sigma_{22} - \sigma_{33})}{2\Delta\sigma}. \qquad [1.50]$$

The parameters σ, $\Delta\sigma$, and η constitute an equivalent description of the shielding tensor as the principal values. Variations in σ due to different electronic environments cause variations in the resonance frequencies of the nuclei. In effect, each nucleus experiences its own local magnetic field. Fluctuations in the local magnetic field as the

molecule rotates results in the CSA relaxation mechanism described in Section 5.4.4.

Resonance frequencies are directly proportional to the static field, B_0; consequently, the difference in chemical shift between two resonance signals measured in frequency units *increases* with B_0. In addition, the absolute value of the chemical shift of a resonance is difficult to determine in practice because B_0 must be measured very accurately. In practice, chemical shifts are measured in *parts per million* (ppm, or δ) relative to a reference resonance signal from a standard molecule:

$$\delta = \frac{\Omega - \Omega_{\text{ref}}}{\omega_0} \times 10^6 = (\sigma_{\text{ref}} - \sigma) \times 10^6, \qquad [1.51]$$

in which Ω and Ω_{ref} are the offset frequencies of the signal of interest and the reference signal, respectively. Chemical shift differences measured in parts per million are independent of the static magnetic field strength so that, for example, all else being equal, chemical shifts reported from experiments on a 500-MHz spectrometer will be the same as those determined on an 800-MHz spectrometer. Referencing of NMR spectra is discussed in detail in Section 3.6.3.

Observed chemical shifts in proteins commonly are partitioned into the sum of two components: the so-called random coil chemical shifts, δ_{rc}, and the conformation-dependent secondary chemical shifts, $\Delta\delta$. The random coil chemical shift of a nucleus in an amino acid residue is the chemical shift that is observed in a conformationally disordered peptide (*22–27*). The secondary chemical shift contains the contributions from secondary and tertiary structures. This distinction is useful because secondary chemical shifts display characteristic patterns for secondary structural elements (*28–32*) and other motifs (*33*) that can provide important structural information and constraints for proteins (*34–40*). In addition, theoretical treatments (*41–46*) are becoming increasingly accurate in predicting protein chemical shifts and chemical shift anisotropies. Distributions of chemical shifts observed in proteins (*47*) are presented in Chapter 9.

1.6 Scalar Coupling and Limitations of the Bloch Equations

A brief treatment of a phenomenon of great practical importance, which will be discussed throughout this text, will be used to illustrate the deficiencies of the Bloch theory. High-resolution NMR spectra of

liquids reveal fine structure due to interactions between the nuclei. However, the splitting of the resonance signals into multiplets is not caused by *direct* dipolar interactions between magnetic dipole moments. Such *dipolar coupling*, although extremely important in solids, is an anisotropic quantity that is averaged to zero to first order in isotropic solution (second-order effects are discussed in Chapter 5). Ramsey and Purcell suggested that the interaction is mediated by the electrons forming the chemical bonds between the nuclei (*48*). This interaction is known as *spin–spin coupling* or *scalar coupling*. The strength of the interaction is measured by the scalar coupling constant, ${}^{n}J_{ab}$, in which n designates the number of covalent bonds separating the two nuclei, a and b. The magnitude of ${}^{n}J_{ab}$ is usually expressed in Hertz and the most important scalar coupling interactions in proteins have $n=1$ to 4. In the present text, n will be written explicitly only if the intended value of n is not clear from the context.

Scalar coupling modifies the energy levels of the system, and the NMR spectrum is modified correspondingly. The prototypical example consists of two spin-1/2 nuclei (e.g., two ^{1}H spins or an ^{1}H spin and a ^{13}C spin). The two spins are designated I and S. The resonance frequencies are ω_I and ω_S, respectively,

$$\omega_I = -\gamma_I B_0(1-\sigma_I), \qquad \omega_S = -\gamma_S B_0(1-\sigma_S). \tag{1.52}$$

The magnetic quantum numbers are m_I and m_S; each spin has *two* stationary states that correspond to the magnetic quantum numbers $1/2$ and $-1/2$. The complete two-spin system is described by *four* wavefunctions corresponding to all possible combinations of m_I and m_S,

$$\begin{aligned} \psi_1 &= \psi\left(\tfrac{1}{2},\tfrac{1}{2}\right), & \psi_2 &= \psi\left(\tfrac{1}{2},-\tfrac{1}{2}\right), \\ \psi_3 &= \psi\left(-\tfrac{1}{2},\tfrac{1}{2}\right), & \psi_4 &= \psi\left(-\tfrac{1}{2},-\tfrac{1}{2}\right), \end{aligned} \tag{1.53}$$

where the first quantum number describes the state of the I spin and the second describes the S spin. In the absence of scalar coupling between the spins, the energies of these four states are the sums of the energies for each spin. Remembering that the β state has a higher (lower) energy compared to the α state for positive (negative) γ, the energies are found to be

$$\begin{aligned} E_1 &= \tfrac{1}{2}\hbar\omega_I + \tfrac{1}{2}\hbar\omega_S, & E_2 &= \tfrac{1}{2}\hbar\omega_I - \tfrac{1}{2}\hbar\omega_S, \\ E_3 &= -\tfrac{1}{2}\hbar\omega_I + \tfrac{1}{2}\hbar\omega_S, & E_4 &= -\tfrac{1}{2}\hbar\omega_I - \tfrac{1}{2}\hbar\omega_S. \end{aligned} \tag{1.54}$$

The total magnetic quantum number m for each energy level is the sum of the individual terms

$$\begin{aligned} m_1 &= +\tfrac{1}{2}+\tfrac{1}{2} = +1, \qquad & m_2 &= +\tfrac{1}{2}-\tfrac{1}{2} = 0, \\ m_3 &= -\tfrac{1}{2}+\tfrac{1}{2} = 0, \qquad & m_4 &= -\tfrac{1}{2}-\tfrac{1}{2} = -1. \end{aligned} \tag{1.55}$$

The energy level diagram for a two-spin system with $\gamma_I > \gamma_S > 0$ is shown in Fig. 1.7a. The observable transitions obey the selection rule $\Delta m = \pm 1$. Therefore, the allowed transitions occur between states 1–2, 3–4, 1–3, and 2–4 in Fig. 1.7; transitions between 2–3 or 1–4 are

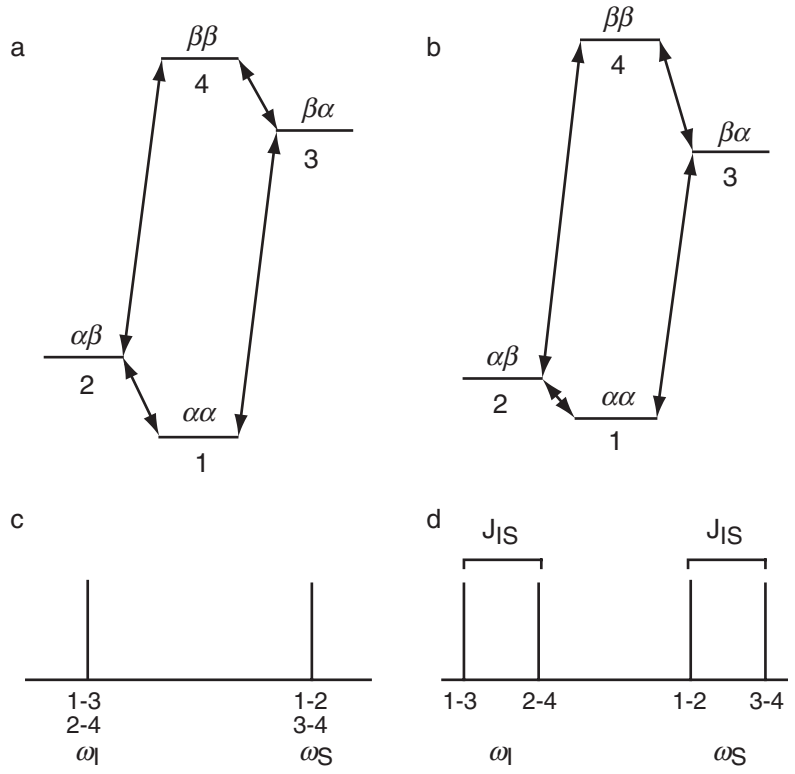

FIGURE 1.7 Energy levels for an AX spin system. Shown are the energy levels for an AX spin system in the (a) absence and (b) presence of scalar coupling interactions between the spins, assuming $J_{IS} > 0$ and $\gamma_I > \gamma_S > 0$. The allowed transitions are indicated between arrows. The energies of the four spins states are defined by (a) [1.54] and (b) [1.56].

forbidden. The first two transitions involve a change in the spin state of the S spin while the latter two involve a change in the spin state of the I spin. Consequently, the NMR spectrum shown in Fig. 1.7c consists of one resonance line at ω_I, due to transitions 1–3 and 2–4, and one resonance line at ω_S, due to transitions 1–2 and 3–4.

Introducing the scalar coupling between I and S, with a value of J_{IS}, modifies the energy levels to

$$\begin{aligned} E_1 &= \tfrac{1}{2}\hbar\omega_I + \tfrac{1}{2}\hbar\omega_S + \tfrac{1}{2}\pi\hbar J_{IS}, \qquad & E_2 &= \tfrac{1}{2}\hbar\omega_I - \tfrac{1}{2}\hbar\omega_S - \tfrac{1}{2}\pi\hbar J_{IS}, \\ E_3 &= -\tfrac{1}{2}\hbar\omega_I + \tfrac{1}{2}\hbar\omega_S - \tfrac{1}{2}\pi\hbar J_{IS}, \qquad & E_4 &= -\tfrac{1}{2}\hbar\omega_I - \tfrac{1}{2}\hbar\omega_S + \tfrac{1}{2}\pi\hbar J_{IS}, \end{aligned} \tag{1.56}$$

in which weak coupling has been assumed with $2\pi|J_{IS}| \ll |\omega_I - \omega_S|$. These expressions are derived from the following equation (see Section 2.5.2):

$$E(m_I, m_S) = m_I\omega_I + m_S\omega_S + 2\pi m_I m_S J_{IS}. \tag{1.57}$$

The term in J_{IS} depends on the spin states of both nuclei but the terms in ω_I and ω_S depend on the spin state of a single nucleus. The energy level diagram for a scalar coupled two-spin system is shown in Fig. 1.7b, assuming that $J_{IS} > 0$. The resulting effect in the spectrum of the scalar coupled system is easily seen from the new values from the transition frequencies,

$$\begin{aligned} \omega_{12} &= \omega_S + \pi J_{IS}, \qquad & \omega_{34} &= \omega_S - \pi J_{IS}, \\ \omega_{13} &= \omega_I + \pi J_{IS}, \qquad & \omega_{24} &= \omega_I - \pi J_{IS}. \end{aligned} \tag{1.58}$$

Now the spectrum shown in Fig. 1.7d consists of *four* lines: two centered around the transition frequency, ω_S, of the S spin but separated by $2\pi J_{IS}$, and two centered around the transition frequency of the I spin, ω_I, but separated by $2\pi J_{IS}$. A weakly coupled two-spin system is referred to as an AX spin system and a strongly coupled two-spin system is referred to as an AB spin system, in which A and X or A and B represent the pair of scalar coupled spins.

The Bloch vector model of NMR phenomena predicts that two resonance signals will be obtained for the two-spin system; in actuality, if the two spins share a nonzero scalar coupling interaction, then four resonance signals are obtained. The basic Bloch model can be extended to describe the evolution of a scalar coupled system by treating each resonance line resulting from the scalar coupling interaction as an independent magnetization vector in the rotating frame. Although additional insights can be gained from using this approach, many problems still arise: (*i*) strong coupling effects that occur when

$2\pi J_{IS} \approx |\omega_I - \omega_S|$ cannot be described, (*ii*) the results of applying nonselective pulses to transverse magnetization in a homonuclear coupled system cannot be described without introducing additional *ad hoc* assumptions, and (*iii*) transfer of magnetization via forbidden transitions when the spin system is not at equilibrium cannot be explained.

In principle, the Bloch picture is strictly only applicable to a system of noninteracting spin-1/2 nuclei. Despite these limitations, the Bloch model should not be abandoned completely. Many of the concepts and much of the terminology introduced by this model appear throughout the whole of NMR spectroscopy. Although the Bloch model is a valuable tool with which to visualize simple NMR experiments, more rigorous approaches are necessary to describe the gamut of modern NMR techniques. Much of the remaining theory presented in this text is devoted to developing methods of analysis that accurately predict the behavior of systems of two or more nuclear spins that interact via scalar coupling or other interactions.

References

1. R. R. Ernst, W. A. Anderson, *Rev. Sci. Instrum.* **37**, 93–102 (1966).
2. J. Jeener, Ampère Summer School, Basko Polje, Yugoslavia (1971).
3. J. Jeener, in "NMR and More. In Honour of Anatole Abragam" (M. Goldman, M. Porneuf, eds.), pp. 1–379. Les Editions de Physique, Les Ulis, France, 1994.
4. R. R. Ernst, *Angew. Chem., Int. Eng. Ed.* **31**, 805–930 (1992).
5. K. Wüthrich, *Angew. Chem., Int. Eng. Ed.* **42**, 3340–3363 (2003).
6. F. Bloch, W. W. Hansen, M. Packard, *Phys. Rev.* **69**, 127 (1946).
7. E. M. Purcell, H. C. Torrey, R. V. Pound, *Phys. Rev.* **69**, 37–38 (1946).
8. T. Sloan, *Phil. Trans. R. Soc. Lond., Ser. A* **359**, 379–389 (2001).
9. K. Rith, A. Schafer, *Sci. Am.* **281**, 58–63 (1999).
10. E. Merzbacher, "Quantum Mechanics," 2nd edn., pp. 1–621. Wiley & Sons, New York, 1970.
11. F. Bloch, *Phys. Rev.* **70**, 460–474 (1946).
12. H. Goldstein, "Classical Mechanics," 2nd edn., pp. 1–672. Addison-Wesley, Reading, MA, 1980.
13. M. H. Levitt, *J. Magn. Reson.* **126**, 164–182 (1997).
14. D. I. Hoult, N. S. Ginsberg, *J. Magn. Reson.* **148**, 182–199 (2001).
15. D. I. Hoult, B. Bhakar, *Concepts Magn. Reson.* **9**, 277–297 (1997).
16. R. R. Ernst, G. Bodenhausen, A. Wokaun, "Principles of Nuclear Magnetic Resonance in One and Two Dimensions," pp. 1–610. Clarendon Press, Oxford, 1987.
17. P. L. Corio, "Structure of High-resolution NMR Spectra," pp. 1–548. Academic Press, New York, 1967.
18. C. Counsell, M. H. Levitt, R. R. Ernst, *J. Magn. Reson.* **63**, 133–141 (1985).
19. R. C. Cantor, P. R. Schimmel, "Biophysical Chemistry," pp. 1–1371. W. H. Freeman, San Francisco, 1980.

20. R. M. Venable, R. W. Pastor, *Biopolymers* **27**, 1001–1014 (1988).
21. D. M. Schneider, M. J. Dellwo, A. J. Wand, *Biochemistry* **31**, 3645–3652 (1992).
22. R. Richarz, K. Wüthrich, *Biopolymers* **17**, 2133–2141 (1978).
23. D. Braun, G. Wider, K. Wüthrich, *J. Am. Chem. Soc.* **116**, 8466–8469 (1994).
24. A. Bundi, K. Wüthrich, *Biopolymers* **18**, 285–297 (1979).
25. G. Merutka, H. J. Dyson, P. E. Wright, *J. Biomol. NMR* **5**, 14–24 (1995).
26. S. Schwarzinger, G. J. A. Kroon, T. R. Foss, J. Chung, P. E. Wright, H. J. Dyson, *J. Am. Chem. Soc.* **123**, 2970–2978 (2001).
27. D. S. Wishart, C. G. Bigam, A. Holm, R. A. Hodges, B. D. Sykes, *J. Biomol. NMR* **5**, 67–81 (1995).
28. D. S. Wishart, B. D. Sykes, F. M. Richards, *J. Mol. Biol.* **222**, 311–333 (1991).
29. A. Pastore, V. Saudek, *J. Magn. Reson.* **90**, 165–176 (1990).
30. M. P. Williamson, *Biopolymers* **29**, 1423–1431 (1990).
31. A. Pardi, G. Wagner, K. Wüthrich, *Eur. J. Biochem.* **137**, 445–454 (1983).
32. S. Spera, A. Bax, *J. Am. Chem. Soc.* **113**, 5490–5492 (1991).
33. A. M. Gronenborn, G. M. Clore, *J. Biomol. NMR* **4**, 455–458 (1994).
34. G. Cornilescu, F. Delaglio, A. Bax, *J. Biomol. NMR* **13**, 289–302 (1999).
35. J. Kuszewski, J. Qin, A. M. Gronenborn, G. M. Clore, *J. Magn. Reson., Ser. B* **106**, 92–96 (1995).
36. D. S. Wishart, D. A. Case, *Meth. Enzymol.* **338**, 3–34 (2001).
37. D. S. Wishart, B. D. Sykes, *Meth. Enzymol.* **239**, 363–392 (1994).
38. D. S. Wishart, B. D. Sykes, F. M. Richards, *Biochemistry* **31**, 1647–1651 (1992).
39. P. Luginbühl, T. Szyperski, K. Wüthrich, *J. Magn. Reson., Ser. B* **109**, 229–233 (1995).
40. R. D. Berger, P. H. Bolton, *J. Biomol. NMR* **10**, 129–142 (1997).
41. D. Sitkoff, D. A. Case, *Prog. NMR Spectrosc.* **32**, 165–190 (1998).
42. A. C. de Dios, J. G. Pearson, E. Oldfield, *Science* **260**, 1491–1496 (1993).
43. X. P. Xu, D. A. Case, *J. Biomol. NMR* **21**, 321–333 (2001).
44. E. Oldfield, *Annu. Rev. Phys. Chem.* **53**, 349–378 (2002).
45. X. P. Xu, D. A. Case, *Biopolymers* **65**, 408–423 (2002).
46. S. Neal, A. M. Nip, H. Zhang, D. S. Wishart, *J. Biomol. NMR* **26**, 215–240 (2003).
47. H. Zhang, S. Neal, D. S. Wishart, *J. Biomol. NMR* **25**, 173–195 (2003).
48. N. F. Ramsey, E. M. Purcell, *Phys. Rev.* **85**, 143–144 (1952).
49. A. G. Palmer, J. Cavanagh, P. E. Wright, M. Rance, *J. Magn. Reson.* **93**, 151–170 (1991).